CFD Prediction of Turbulent Flow on an Experimental Tidal Stream Turbine using RANS modelling

CFD Prediction of Turbulent Flow on an Experimental Tidal Stream Turbine using RANS modelling

James McNaughton[1,#], Stefano Rolfo[1], David Apsley[1], Imran Afgan[1,2], Peter Stansby[1] and Tim Stallard[1]

1 School of Mechanical Aerospace and Civil Engineering, University of Manchester, Sackville Street, Manchester, M1 3BB, England
2 Institute of Avionics & Aeronautics, Air University, E-9, Islamabad, Pakistan
Corresponding Author / E-mail: james.mcnaughton@postgrad.manchester.ac.uk, TEL: +44-7772-533014

KEYWORDS : Computational Fluid Dynamics (CFD), Reynolds Averaged Navier Stokes (RANS), Tidal energy, Tidal stream turbine (TST), ReDAPT

A detailed computational fluid dynamics (CFD) study of a laboratory scale tidal stream turbine (TST) is presented. Three separate Reynolds Averaged Navier Stokes (RANS) models: the $k-\varepsilon$ and $k-\omega$ SST eddy-viscosity models, and the Launder-Reece-Rodi (LRR) Reynolds stress model, are used to simulate the turbulent flow-field using a new sliding-mesh method implemented in EDF's open-source Computational Fluid Dynamics solver, Code_Saturne. Validation of the method is provided through a comparison of power and thrust measurements for varying tip-speed ratios (TSR). The SST and LRR models yield results within several per cent of experimental values, whilst the k-ε model significantly under-predicts the force coefficients. The blade and turbine performance for each model is examined to identify the quality of the predictions. Finally, detailed modelling of the turbulence and velocity in the near and far wake is presented. The SST and LRR models are able to identify tip vortex structures and effects of the mast as opposed to the standard $k-\varepsilon$ model.

NOMENCLATURE

A	= Swept area of turbine (m^2)
$C_{T/P}$	= Thrust (T) / Power (P) coefficients
$\bar{C}$	= Time-averaged coefficient
$\tilde{C}$	= Phase-averaged coefficient
C'	= RMS of $\bar{C}$
C^*	= RMS of $\tilde{C}$
C_μ	= Constant
I	= Turbulent intensity
k	= Turbulent kinetic energy (m^2s^{-2})
L	= Turbulent length scale (m)
R	= Turbine blade radius (m)
TSR	= Tip-speed-ratio
U_0	= Inflow velocity (ms^{-1})
y^+	= Non-dimensional wall distance of mesh
ε	= Turbulent dissipation rate ($m^2 s^{-3}$)
ρ	= Fluid density ($kg\ m^{-3}$)
ϕ_i	= Value of variable ϕ at cell i
ω	= Specific rate of turbulent dissipation (s^{-1})
Ω	= Angular velocity of turbine ($rad\ s^{-1}$)

1. Introduction

Interest in renewable energy has come into the forefront over the last decade due to concerns of diminishing oil and coal supplies as well as from worldwide political pressures to "go green". Tidal currents provide the opportunity to extract energy from a powerful and predictable resource. One method of energy extraction from tidal currents is to use a tidal stream turbine (TST). A report by the European Commission (1996) identified numerous tidal sites with an estimated power rating exceeding 10MW per square km. The Orkneys, off the north coast of Scotland, are among these power-rich sites and home to the European Marine Energy Centre (EMEC). Osalusi *et al.* (2009) show that currents at the EMEC test site are highly turbulent with mean velocities greater than 1m/s, meaning TSTs experience strong and unsteady loading. To understand the effect of such flow-features, experimental and computational studies are used. Bahaj *et al.* (2005, 2007) present a study of flow past an experimental TST in a towing tank and cavitation tunnel presenting the thrust and power coefficients, C_T, and C_P respectively, against the tip-speed ratio (TSR), which are defined as:

$$\mathrm{TSR} = \frac{\Omega R}{U_0}$$

$$C_T = \frac{\text{Thrust}}{\frac{1}{2}\rho A U_0^2}$$
$$C_P = \frac{\text{Power}}{\frac{1}{2}\rho A U_0^3}$$

Where Ω is the angular velocity of the TST in rad/s, R is the blade radius (m), U_0 is the reference velocity (m s^{-1}), ρ is the fluid density (kg m^{-3}) and $A = \pi R^2$ is the swept area of the turbine (m^2). Whilst these studies provide a large data set for the mean force coefficients, they provide little information about the behaviour in the wake. Indeed, experimentally it is hard to observe the fluid behaviour close to the turbine and therefore modelling can provide further insight in these areas. Blade element / momentum (BEM) methods, originally used in wind-turbine design (Wilson & Lissaman, 1974), divide blades into 2D sections for which drag and lift coefficients are known. BEM methods have been used in TST modelling (eg Batten *et al.* 2008) with results comparable to experimental values. However, BEM is unable to model the more complex flow conditions and reveals no information of unsteady loading or the wake.

Computational fluid dynamics (CFD) is a valuable tool that allows these gaps to be bridged. One common method for CFD analysis of TSTs uses actuator disk theory. In this method the TST is modelled as a porous disk that inflicts a pressure drop as fluid passes through it (eg Gant and Stallard, 2008). Such a method is useful in predicting the far wake, but gives little information close to the turbine, as shown by Harrison *et al.*, (2009). Detailed CFD modelling of Bahaj *et al.'s* TST is demonstrated by McSherry *et al.* (2011) and Afgan *et al.* (2012), which model the turbine's blades and support structure. The first of these studies uses Reynolds Averaged Navier Stokes (RANS) modelling to represent the turbulence, whilst the latter uses Large Eddy Simulation (LES), with both studies predicting power and thrust measurements close to the experimental data. LES is a more computationally expensive method but provides a greater level of detail than RANS. Indeed, the computational mesh used by Afgan et al. has over twenty times more cells than that of McSherry et al.'s and the increase in CPU time is in the order of 100,000's. However, whilst the RANS study only provides details of the power and thrust measurements, the LES provides detailed information in the near wake and on the blade surfaces.

This paper addresses the gap left between the RANS and LES calculations of a TST that are described above. A sliding-mesh method is used to model detailed flow past the experimental model of Bahaj *et al.'s* horizontal-axis TST. Simulations using this geometry are used to assess the suitability of different RANS models with comparisons drawn with the LES of Afgan *et al.* where applicable.

2. Methodology

2.1. Numerical Solver

Simulations are performed using Électricité de France Research and Development's (EDF R&D) open-source CFD solver, *Code_Saturne* (Archambeau, 2004). The code is an unstructured finite volume-code using pressure-velocity coupling through a predictor-corrector scheme. The code is optimised for large parallel calculations (Fournier *et al.*, 2011). Second-order-slope-limited differencing is used in space and first-order implicit Euler scheme is used in time.

2.2. Turbulence models

Three different RANS models are selected for validation of results with the Southampton turbine: the $k-\varepsilon$ (Launder & Sharma, 1974) and $k-\omega$ SST (Menter, 1994) eddy-viscosity models and the Launder-Reece-Rodi (LRR, see Launder *et al.*, 1975) Reynolds Stress Model (RSM). These models are popular, often chosen as industry standards, and typical of those used by previous studies of TSTs (e.g. Mason Jones *et al.*, 2008, O'Doherty *et al.*, 2009, Harrison *et al.*, 2009). RSMs are able to model anisotropy by solving separate transport equations for each of the Reynolds stresses whilst eddy-viscosity models cannot achieve this as they assume that the Reynolds Stress tensor is proportional to the mean strain rate. For this reason it is often observed (for example in Wilcox, 1994) that eddy-viscosity models are not suitable for predicting flows with rotation or strong curvature effects as is expected in the current flow.

2.3. Wall functions

Due to the complex nature of both flow and geometry it is difficult to obtain a near wall cell that is well placed within the laminar sub-layer (i.e. at $y^+ \approx 1$, where y^+ is the dimensionless wall-distance) which is a necessary condition to correctly resolve the boundary layer. Therefore wall-functions are used based on the classical log-law (von Kármán, 1930) with the modification proposed by Grotjans & Menter (1998), known as the scalable wall-function. The advantage of this formulation is that the near wall distance is prevented from falling below a set limit (in *Code_Saturne* this is set at 10.88) so that the near wall cell-centre always lies within the buffer layer, and hence the wall-function's requirements are always satisfied.

2.4. Boundary conditions

To recreate the conditions of the towing tank, slip boundary conditions are placed on the sides, top and bottom walls of the domain. The turbine and its support have no-slip walls. The inlet has a uniform velocity profile with a fixed turbulence intensity of $I = 1\%$. The turbulent kinetic energy (TKE), k, and dissipation rate, ε, are defined at the inlet:

$$k = \frac{3}{2}(IU_0)^2$$
$$\varepsilon = \frac{C_\mu^{\frac{3}{4}} k^{\frac{3}{2}}}{L}$$

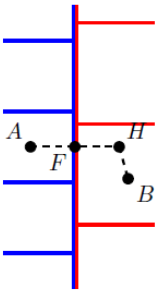

Figure 1. Interpolation of cells for sliding mesh method.

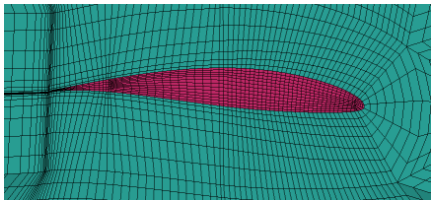

(a) C-mesh (green) and tip mesh (red).

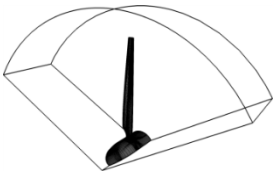

(b) 120° segment.

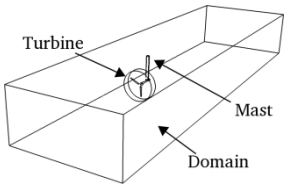

(c) Outline of domain.

Figure 2. Overview of domain and mesh.

$C_\mu = 0.09$ is a constant and L is the turbulent length scale that is given the value of 0.7 times the turbine hub-height, as described in Gant and Stallard (2007). For the $k-\varepsilon$ model these values are prescribed at the inlet whilst for the other models they are used to calculate the required variables from their definitions.

2.5. Sliding mesh

In order to rotate the turbine the mesh is created as two blocks: an outer-stationary and an inner-rotating part. A sliding-mesh approach is developed within *Code_Saturne* as part of this work. The sliding-mesh interface employs an internal Dirichlet boundary condition calculated from a halo-node as in Fig. 1. The value of any variable, ϕ, at face, F, on the sliding-mesh interface is given the value ϕ_F:

$$\phi_F = \frac{\phi_A + \phi_H}{2}$$

Where A is the cell connected to F and H is the halo-point; found by reflecting A through F. The value at H is found by extrapolating from the nearest cell-centre, B, say:

$$\phi_H = \phi_B + \nabla\phi_B \cdot \overrightarrow{BH}$$

2.6. Geometry

The turbine is a 0.8m diameter experimental model whose blades are constructed from seventeen NACA 6-series aerofoil profiles that change in pitch, chord-length and thickness along the blade radius, R. The profiles and all other geometry such as the support are defined in Bahaj *et al.* (2005). A block-structured mesh is used entirely throughout the geometry. A c-mesh is used around the blades as in Fig. 2a. The trailing edges of each profile have been thickened using a function described in Herrig *et al.* (1951) to allow for a more realistic blade design, as well as allowing for the structured mesh at the blade-tip. The near-wall spacing of the mesh is designed to give a y^+ value in the range 15-300 which are suitable for wall-functions. If the value of y^+ falls below 10.88 the scalable wall-function is activated.

The turbine is created in a 120° segment as shown in Fig. 2b and then copied twice around the axis of rotation to create a cylindrical block. This block is housed inside an outer domain shown in Fig. 2c with the turbine and outer blocks communicating via a sliding-mesh method described in Sec. 2.5. The domain matches the depth and breadth of the towing tank in Bahaj *et al.* (2005) with the inlet 5D upstream of the turbine and the outlet 12D downstream.

Table 1 Mean force coefficients for different sizes of meshes.

Mesh	*No cells turbine*	*No cells domain*	*No cells total*	$\overline{C_T}$	$\overline{C_P}$
Coarse	823977	627356	1451333	0.8094	0.4446
Medium	3078636	627356	3705992	0.8270	0.4638
Fine	5336976	627356	5964332	0.8256	0.4651
Medium w/ fine outer	3078636	2395928	5474564	0.8278	0.4635

2.7. Mesh refinement

Convergence of the solution is sought for three levels of meshing (coarse, medium, fine) for the turbine block and two (medium, fine) for the outer domain. These are described in Table 1 alongside the mean thrust and power coefficients obtained using the $k-\omega$ SST model with TSR=6. The fine turbine block changes these values by less than one percent and so this level of refinement is not deemed necessary here and the medium mesh is used. Refining the outer domain again has a negligible effect on the coefficients, implying that this level of refinement in the domain is not necessary to match the force coefficients of the experiments. The effect in the downstream wake is shown by mean velocity profiles in the wake in Fig. 3. At 1D no significant differences are seen between the solutions although the finer mesh identifies more variation in the centre-line of the turbine. At 5D the difference between solutions is again negligible although by 10D the coarser solution has shown a greater wake recovery by around 10% on the centre-line. Hence for studying the wake confidence can be drawn in the near wake solution but further downstream there may be errors arising from the mesh. The simulations use a time-step equivalent to 0.6° of rotation per time-step. Although this is quite low, doubling the time-step affects these results by approximately 8% and so cannot be increased without significantly effecting results.

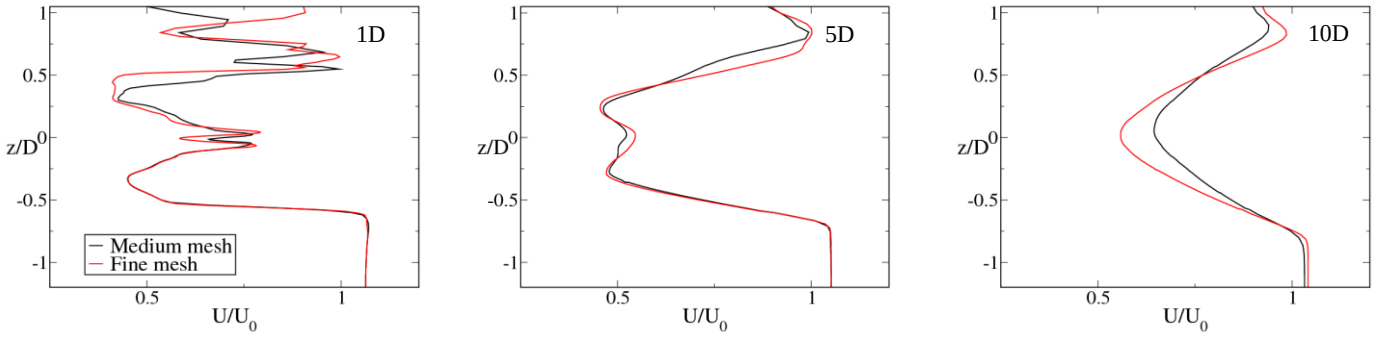

Figure 3. Mean velocity profiles for medium and fine outer domain meshes.

3. Results

Simulations are performed using the University of Manchester's Computational Shared Facility (CSF) with each simulation running on between 32 and 128 cores and taking approximately 20,000 CPU hours for the force coefficients to reach a periodic state. The $k-\varepsilon$ is the least expensive model to run computationally, with the LRR and $k-\omega$ SST models taking approximately two and three times longer, respectively. This is expected for the LRR model which solves transport equations for the Reynolds stresses, whilst the high cost of the SST can be attributed to the requirement to calculate the wall distance at each time-step. To reduce computational cost for the parametric test of TSRs, each simulation is performed in turn restarting from the previous results. The time step is adjusted to give the same angle of rotation per time step. Once a periodic state is achieved for each TSR the calculation is allowed to run for a minimum of three further complete rotations. For further analysis of the optimal TSR these results are averaged over a time corresponding to the fluid travelling from the turbine to the outlet

Fig. 4 shows the instantaneous velocity flow-field for the three models at TSR=6 all captured at approximately the same instant. The SST and LRR models show quite unsteady wakes, especially behind the mast, with the SST model capturing a larger area of recirculation behind the top of the mast. Similarly the velocity deficit from the tip vortices are visible in all three instances, although the $k-\varepsilon$ does not capture this as well as the other models. The simulations take approximately 7 seconds of physical time before reaching a periodic state for the force coefficients. This equates to just less than one full flow-through pass of the domain, approximately 25 rotations of the turbine.

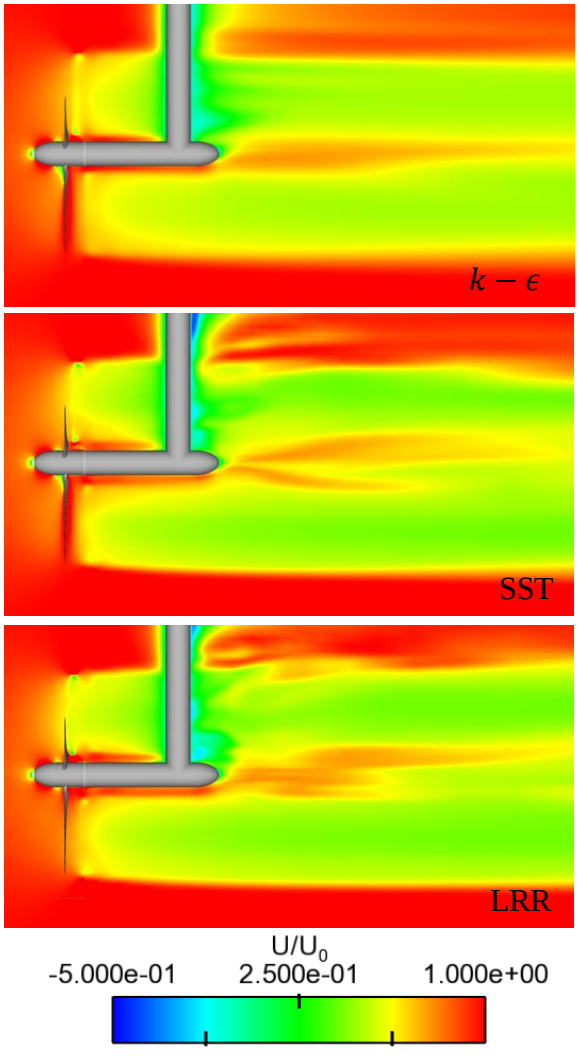

Figure 4. Instantaneous velocity field for different RANS models.

3.1. Comparison to experiments

Thrust and power coefficients as a function of TSR are shown in Fig. 5, comparing the RANS models to the experimental data in Bahaj *et al.* (2007). A blockage correction applied to the experimental data is also applied to the presented results in the graphs. Also shown are the LES results from Afgan *et al.* (2012). All models give their best prediction at TSR=6, with the SST and LRR models also showing favourable results for a TSR of 7. This may be a result of the mesh sensitivity study being performed at this TSR, also near the optimal value flow is likely to be less separated at the blades. As expected the $k-\varepsilon$ model performs poorly, which may reflect the model's less satisfactory performance in separated flows. Over the covered range of TSRs the LRR and SST models both give results

close to the experimental data curves, with the worst agreement at the lowest TSR. Both these models show results within several per cent of the LES, under predicting the $\overline{C_P}$ values slightly but giving better agreement to the experiments for the thrust coefficient.

3.2. Performance characteristics

A better understanding of the different turbulence models' performances is given by the force coefficient behaviour throughout each rotation. Fig. 6a shows several sets of the instantaneous power coefficient plotted over a single rotation. Defining the phase as this time interval, then the phase average, $\widetilde{C_P}$, is obtained by averaging the data points that are at the same point in the phase. Fig. 6b and c also show the normalised phase averaged thrust and power coefficients, $\widetilde{C_T}/\overline{C_P}$ and $\widetilde{C_P}/\overline{C_P}$ respectively, for each of the RANS models. All models experience larger fluctuations for power than thrust indicating a larger unsteadiness for the rotational effects. Further to this there are two frequencies identifiable for each model: the larger of these occurring at the point where a blade is directly in front of the mast, indicated by the zero, one- and two-third points of the phase. For the SST and LRR models interaction with the mast is thus indicated by the maximum and minimum peaks of the coefficients occurring before and after each blade passing respectively. Compared to the LRR models these peaks are smaller for the SST model and are delayed slightly. The $k-\varepsilon$ model predictions are delayed even further, placing it almost in anti-phase to the LRR model, hence predicting maximum values after a blade passes the mast. Whilst the $k-\varepsilon$ and LRR models predict a steady oscillatory motion for their peaks and troughs the SST shows a recovery and stall in the $\widetilde{C_P}$ and $\widetilde{C_T}$ peaks respectively as each blade passes the mast. This shows the SST is predicting a secondary interaction with the mast. Indeed, referring back to Fig. 4 the velocity gradient extending from the join between the mast and the nacelle is greater for the SST model than the other turbulence closures.

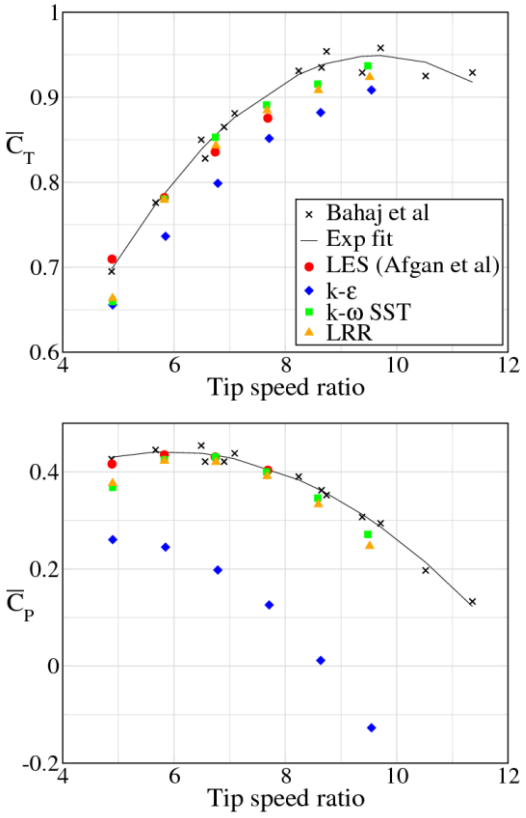

Figure 5. Blockage corrected thrust and power coefficients for different RANS models compared to experimental data.

Root mean square (RMS) fluctuations of each coefficient from the mean, C_P', and from the phase, C_P^*, are defined as:

$$C_P' = \sqrt{\overline{(C_P - \overline{C_P})^2}}$$

$$C_P^* = \sqrt{\overline{\left(C_P - \widetilde{C_P}\right)^2}}$$

These are given in Table 2 which shows the fluctuations from the phase to be around half that of those from the mean for all models identifying that even with this well-defined phase the unsteadiness of the solution is still large. The LRR model's predictions of these fluctuations are almost twice that of the SST and over double the $k-\varepsilon$ model's values. This behaviour may be due to RSMs tending to naturally damp the modelling contribution which allows for a larger amount of the turbulent spectrum to be resolved. This is again observed in the comparison between TKE and resolved velocity

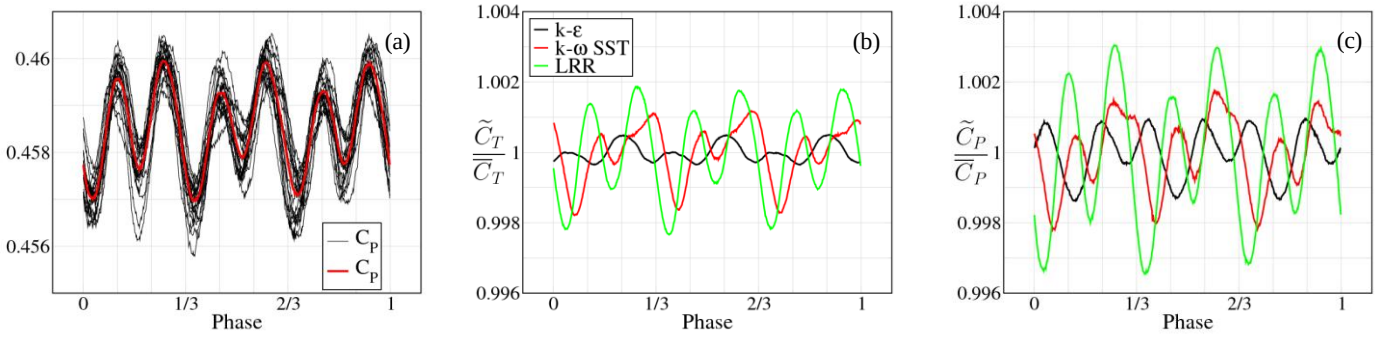

Figure 6. Phase averaging of power coefficient over one rotation. (a) Instantaneous values and their phase average. Normalised phase average of thrust (b) and power (c) for different RANS models.

fluctuations detailed in Sec. 3.3. Whilst the SST is able to accurately predict the mean flow this shows an advantage of the LRR for examining unsteady loads.

A greater understanding of the loading on the blades is obtained from the mean pressure coefficient:

$$\bar{C}_{pres} = \frac{p - p_{ref}}{\frac{1}{2}\rho U_0^2}$$

p_{ref} is the reference pressure taken at the centre point of the inflow boundary. $\bar{C}_{pres}$ is shown at one-quarter lengths along the blade in Fig. 7 as a function of distance, c, along chord length, C. The large variation in the pressure coefficient from root (r/R=0.25) to tip (r/R=0.75) is due to the normalisation only taking into account the inflow velocity as opposed to using the relative velocity based on Ωr, in this manner a better understanding of the forces at each section are given in relation to each other as well as between models. The $k-\varepsilon$ model shows quite different performance characteristics to the other models, this is a direct result of the model's insensitivity to adverse pressure gradients and curvature. At one quarter radius this is observed by the inability to maintain the large suction peak at the leading edge and thus the pressure recovery is quite steep. This characteristic is seen for the other presented sections although is less severe.

The plots at r/R=0.5 exhibit separation for all models in the region $0.2 < c/C < 0.3$, with the SST model predicting this occurrence earliest and the $k-\varepsilon$ the latest. Fig. 2a shows that the blade sections are generally convex, although there is a concave region toward the trailing edge of the pressure surface. This type of curved surfaces lead to reduced and increased turbulence respectively, Out of the turbulence closures chosen in this study, only the LRR model can correctly predict these production levels making it most likely to give an accurate prediction at the blades surfaces. Certainly the boundary layer prediction of ω-based models has low mixing levels which leads to separation whilst the $k-\varepsilon$ model has higher levels of mixing which makes it less likely to predict separation.

The mean blade coefficients are quite similar for the SST and LRR models, with the former showing slightly larger forces on the pressure and suction surfaces higher up the blade length, this accounts for the marginal increase in force coefficients. The greatest difference between these models is at r/R=0.25 where the LRR shows a larger suction peak which is maintained further along the blade (see Fig. 7), although being closer to the blade root this has less effect on the overall results.

Table 2 RMS fluctuations of force coefficients from mean and phase averaged values.

	$\overline{C_T}$	C_T'	C_T^*	$\overline{C_P}$	C_P'	C_P^*
KE	0.7750	4.8E-3	9.5E-4	0.2643	4.7E-3	1.8E-3
KW	0.8270	1.7E-2	5.9E-3	0.4638	1.3E-2	5.8E-3
LRR	0.8260	2.6E-2	1.1E-2	0.4613	2.3E-2	1.1E-2

3.3. Wake modelling

Fig. 8 shows mean velocity and TKE on the centre-line downstream of the nacelle. Immediately behind the nacelle (x/D=0.8) the $k-\varepsilon$ and LRR models show a larger peak in velocity than the SST model which is due to the latter giving less mixing in the wake. Indeed at this point the TKE is increasing for the SST model whilst decreasing for the other models. Further analysis of the wake is shown in Fig. 9, which shows vertical velocity profiles at 1, 2, 5 and 10D downstream of the turbine. The SST and LRR models show a greater sensitivity to the mast than the $k-\varepsilon$ model. In the wake of the tip all models show the interaction between the blades and the mast by the non-symmetrical profile. At 2 and 5D downstream the $k-\varepsilon$ model shows the fastest recovery which is a result of the model having the greatest mixing levels. Although by 10D the LRR model has recovered fastest of all models showing by this distance it has experienced a larger level of mixing.

Fig. 10 shows time-averaged TKE (modelled turbulence) and resolved velocity fluctuations, $\frac{1}{2}(\overline{u_i^2} - \overline{u_i}^2)$, in the wake at several downstream locations. Note that for the planes at 0.1R the circular region is inside the turbine mesh and hence rotates in time, which explains the discontinuity over the interface for averaged quantities. Where little modelling occurs more unsteady features, such as those from the tip-vortex interaction with the mast, are captured. Whilst the $k-\varepsilon$ model predicts turbulence in a large region of the flow the LRR model, and to a lesser extent the SST model, resolve the velocity fluctuation which leads to their better comparison with the experimental results. At 0.1R downstream the resolved velocity fluctuations for each model identify tip vortices indicating this is a highly unsteady region. Further downstream the resolved velocity fluctuations identify the effects of the mast. Although the $k-\varepsilon$ model is less sensitive to this due to the higher levels of TKE production, the LRR and SST models both capture tip vortices at 1

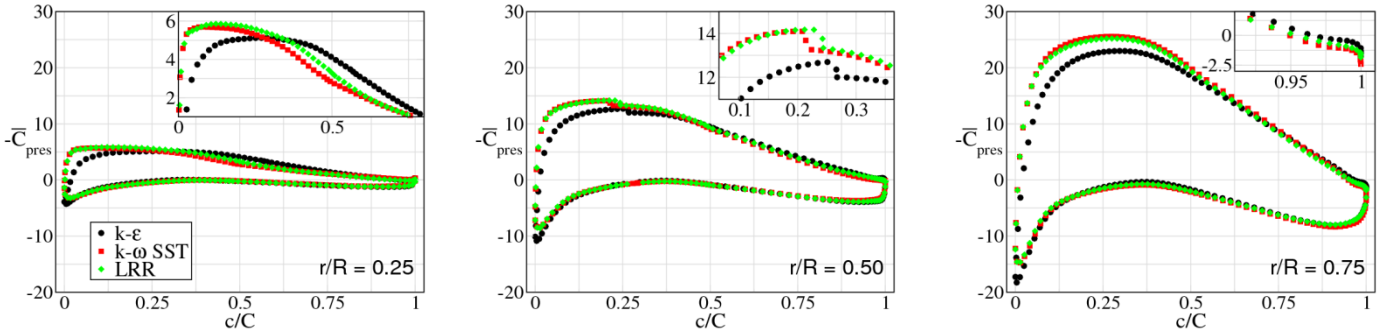

Figure 7. Pressure coefficient at quarter lengths along the blade.

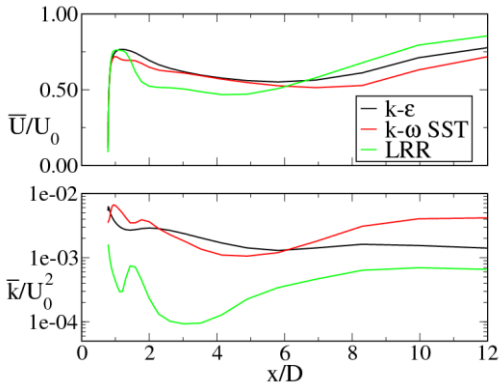

Figure 8. Velocity and TKE in the centre-line wake downstream of the turbine.

and 2D locations. These vortices have an anti-clockwise rotation when looking into the planes in Fig. 10; this rotation is identified by the LRR and SST models' levels of resolved velocity fluctuations as these spiralling vortices interact with the wake of the mast. At 5D the LRR model shows a much larger region of resolved velocity fluctuations than either of the other models due to the rotational effects mixing the turbulent quantities from upstream.

4. Conclusions

This paper demonstrates the ability of three RANS models to model turbulent flow past a TST using an open-source CFD code with a sliding-mesh method. The models chosen are used commonly in industrial design. The mesh study shows that reasonably large cell counts are required to achieve grid convergence. The mesh in the outer domain is shown to be less sensitive to increased resolution for force coefficients. It may be desirable to investigate the required refinement in the wake, or indeed the requisite to correctly model the support structure which would greatly simplify the modelling. Due to the mesh sizes the calculations require a large amount of computational resources. Hence the methodology here is more suited to detailed analysis of flow fields than large parametric studies.

For a range of TSRs the SST model gives results closest to experiments. Near the optimal TSR the values are within experimental spread, whereas for larger TSRs the model tends to under-predict the force coefficients. The LRR model gives force coefficient predictions below that of the SST, while showing greater fluctuations in the instantaneous values. The $k-\varepsilon$ model performs poorly and is shown to be unsuitable for modelling this complex flow. The SST and LRR models match the power prediction of the LES by Afgan *et al.* well and show an improved prediction of the thrust coefficients. In the wake, the SST and LRR models identify greater turbulent structures in the form of the tip vortices and rotation than the $k-\varepsilon$ model which is again attributed to the $k-\varepsilon$ model's shortcomings. However, the similarity in results from SST and LRR models show that an eddy-viscosity model can be used to model the rotational effects in the wake in a similar fashion to the RSM. No high quality experimental or LES data is available in the wake to compare to and so comparison can only be drawn between the models. Hence it is the authors' intention to perform high-quality LES to demonstrate the advantages and disadvantages of the RANS models

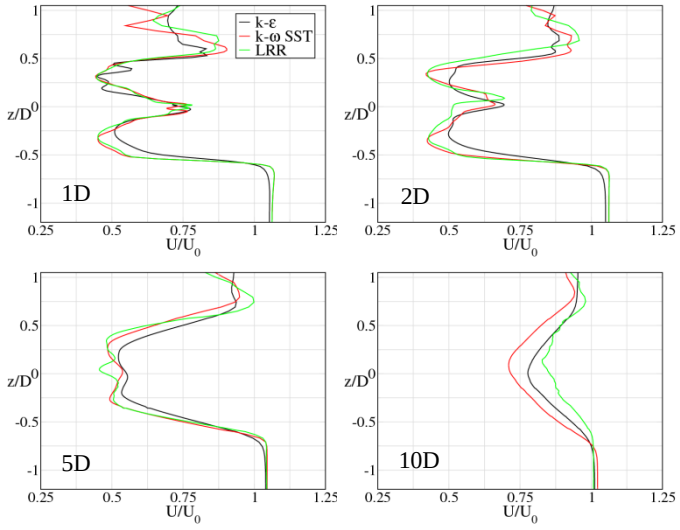

Figure 9. Mean velocity profiles for medium and fine outer domain meshes.

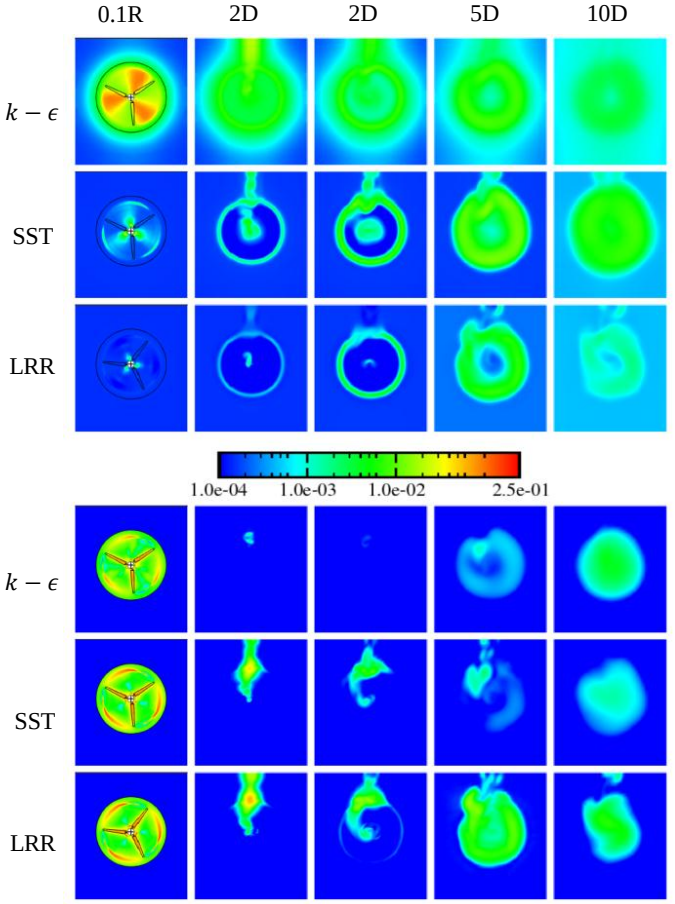

Figure 10. Time-averaged velocity fluctuations on downstream planes normalised by U_0^2. (a) Modelled by turbulence $(\bar{k}/U_0^2)$. (b) Resolved from ensemble mean $\left((\overline{u_i^2}-\overline{u_i}^2)/U_0^2\right)$

for the tidal industry.

The purpose of this work is to identify suitable methodology and RANS models for analysis of Tidal Generation Ltd's 1MW TST that is installed at EMEC. The flow speeds used for the experiment are similar to those of the EMEC test site; hence the Reynolds number will increase linearly with the increase in diameter. Full-scale devices are also subject to substantial velocity shear, greater turbulence intensities and wave-induced fluctuations. Future work will investigate these effects using the methods described here.

ACKNOWLEDGEMENT

This research was performed as part of the Reliable Data Acquisition Platform for Tidal (ReDAPT) project commissioned and funded by the Energy Technologies Institute (ETI). The authors would like to acknowledge the assistance given by IT services at The University of Manchester.

REFERENCES

1. European Commission. Non-nuclear energy Joule II Wave Energy Project Results. "The exploitation of tidal marine currents." European Commission DG Sci [Rep. EUR 16683 EN], 1996.

2. Osalusi E, Side J, Harris R. "Structure of turbulent flow in EMEC ' s tidal energy test site," Int. Communications in Heat and Mass Transfer, Vol. 36, No. 5, pp.422-431, 2009.

3. Bahaj AS, Batten WMJ, Molland AF, Chaplin JR. "Experimental investigation into the effect of rotor blade sweep on the performance of the Marine Current Turbines," Proc. of the Institution of Mechanical Engineers, Part A: Journal of Power and Energy. Vol. 215, No. 5, pp. 611-622, 2005.

4. Bahaj AS, Molland AF, Chaplin JR, Batten WMJ. "Power and thrust measurements of marine current turbines under various hydrodynamic flow conditions in a cavitation tunnel and a towing tank." Renewable Energy. Vol. 32, No. 3, pp. 407-426, 2007.

5. Wilson RE, Lissaman PBS. "Applied aerodynamics of wind power machines." Oregon State Univ., NTIS PB 238594, 1974.

6. Batten WMJ, Bahaj AS, Molland AF, Chaplin JR. "The prediction of the hydrodynamic performance of marine current turbines." Renewable Energy. Vol. 33, pp. 1085-1096, 2008.

7. Gant S, Stallard T. "Modelling a Tidal Turbine in Unsteady Flow." In: Proc. of the Eighteenth (2008) Int. Offshore and Polar Engineering Conference, pp. 473-479, 2008.

8. Harrison ME, Batten WMJ, Myers LE, Bahaj AS. "A comparison between CFD simulations and experiments for predicting the far wake of horizontal axis tidal turbines." In: Proc. of the 8th European Wave and Tidal Energy Conference, Uppsala, Sweden. pp. 566-571, 2009.

9. Mcsherry R, Grimwade J, Jones I, Mathias S, Wells A, Mateus A. "3D CFD modelling of tidal turbine performance with validation against laboratory experiments." In: Proc. 9th European Wave and Tidal Energy Conference, University of Southampton, UK, 2011.

10. Afgan I, McNaughton J, Apsley DD, Rolfo S, Stallard T, St ansby PK. "Large-Eddy Simulation of a 3-bladed horizontal axis tidal stream turbine: comparisons to RANS and experiments." In: Turbulence, Heat and Mass Tr ansfer 7, 2012.

11. Launder BE, Sharma, BI. "Application of the Energy Dissipation Model of Turbulence to the Calculation of Flow near a Spinning Disc." Letters in Heat and Mass Transfer. Vol. 1, No. 2, pp. 131-138, 1974.

12. Menter FR. "Two-Equation Eddy-Viscosity Turbulenc e Models for Engineering Applications." AIAA. Vol. 32, No. 8, pp. 1598-1605, 1994.

13. Launder BE, Reece GJ, Rodi W. "Progress in the de velopment of a Reynolds stress turbulence closure. Jo urnal of Fluid Mechanics." Vol. 68, pp. 537-566, 19 75.

14. Mason-Jones A, O'Doherty T, O'Doherty DM, Wooldridge CF. "Characterisation of a HATT using CFD and ADCP site data." In: ECOR Symposium 2008 and Ocean Innovation 2008 Conference and Exhibition, St John's Newfoundland, 2008.

15. O'Doherty T, Egarr DA, Mason-Jones A, O'Doherty DM. "An assessment of axial loading on a five-turbine array." Proc. of the Institution of Civil Engineers Energy. Vol. 162 No. EN2, pp. 57-65, 2009.

16. Wilcox DC. Turbulence "Modeling for CFD." 2nd ed. DCW Industries, Inc.; 1994.

17. Von Kármán T. "Mechanical Similitude and Turbulence," NACA-TM-611, 1930.

18. Grotjans H, Menter FR. "Wall functions for industrial applications." In: Proc. Of Computational Fluid Dynamics '98, Chichester, UK, ECCOMAS, Vol. 1, No. 2, pp. 1112-1117, 1998.

19. Archambeau F, Mechitoua N, Sakiz M. "*Code_Saturne:* a finite volume code for the computation of turbulent incompressible flows-industrial applications." Int. Journal on Finite Volumes. Vol. 1, No.1, pp. 1–62, 2004.

20. Fournier Y, Bonelle J, Moulinec C, Shang Z, Sunderland AG, Uribe JC. "Optimizing *Code_Saturne* computations on Petascale systems." Computers & Fluids. Vol. 45, No. 1, pp. 103-108, 2011.

21. Herrig J, Emery JC, Erwin JR. "Effect of Section Thickness and Trailing Edge Radius on the Performance of NACA 65-Series Compressor Blades in Cascade at Low Speeds." NASA-RM L51J16. Vol. 29, No. 4, pp. 1-66, 1951.